

NUMERICAL AND EXPERIMENTAL INVESTIGATIONS OF CRF WITH SIMULATION OF FLOW NON-UNIFORMITY IN THE BASIC FLIGHT CONDITIONS

I.A. Brailko, V.I. Milesin, A.M. Volkov, V.N. Korznev
 Central Institute of Aviation Motors (CIAM)
 2, Aviamotornaya St., 111116, Moscow, RUSSIA
 E-mail: milesin@ciam.ru

Keywords: counter rotating fan, inlet distortion, test results

Abstract

The effect of flow non-uniformity at the powerplant inlet of a new-generation aircraft is studied by numerical and experimental investigations of CRF with simulation of the basic flight conditions. All basic characteristics of the fan along the operating line are found within rotation speeds $N_{av} = 50\% - 95\%$ and at rated values of $N2/N1$. The experimental data show that there are no changes in total pressure ratio, π^*_f , at the same rotational speed for uniform and non-uniform flow at the inlet. In this case total air flow, G_{cor} , in the fan model decreases by 1-1.5 kg/s. There is an increase in total pressure ratio in the fan by 1.5-2.0 %, and a decrease in adiabatic efficiency, η^*_{ad} , of the fan model by 1.0-2.0 % at the same airflow in non-uniform flow.

Introduction

In the development of an advanced competitive aircraft of a new generation with a high technical and economic and acoustic efficiency it is necessary to ensure an accurate airframe - powerplant integration for a non-conventional power plant configuration with a counter-rotating fan (CRF). Quality of airflow at the powerplant inlet depends on this integration. Flow non-uniformity arising in flight at the engine inlet can exert a considerable effect on CRF performances. For estimation of these effects experimental investigations are required. These studies have been completed at CIAM's C-3A test facility [1-4]. Characteristics of CRF1

model developed by CIAM were studied. The basic characteristics of CRF with a uniform flow field at the inlet were found at the first stage of this research work. Flow non-uniformity in the fan air intake duct was simulated at the second stage of investigations. This work shows test results and effects of inlet flow distortion on aerodynamic characteristics of CRF1 fan model.

Nomenclature

$W = \Delta\sigma_0 + \varepsilon$ - Total inlet flow distortion
 $\Delta\sigma_0$ – conventional circumferential distortion of quasi-stationary non uniform flow;
 ε – dimensionless intensity of unsteady flow pulsations;
 π^* – total pressure ratio;
 η^*_{ad} – adiabatic efficiency;
 G_{cor} – corrected air flow;
 λ – flow velocity coefficient relatively to critical sound speed

1 Test object

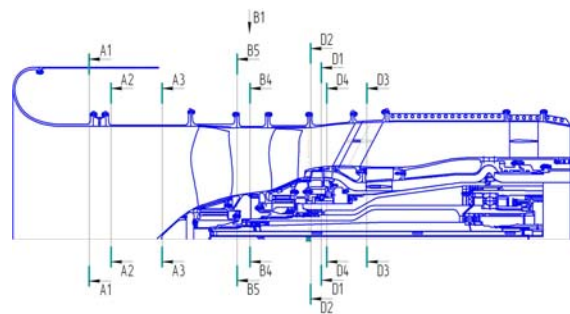


Fig. 1. General view of the fan with the air intake and the flow non uniformity simulator

(Section A2) with the nominal nozzle at the by-pass duct outlet ($D_n=603$ mm)

The CRF 1 fan model consists of two rotors (R1 and R2) and one rotor of the booster stage (RB) with a IGV at its inlet. The non-uniform flow simulator is installed in the intake duct at R1 inlet (the duct diameter is $D_{A2} = 558.8$ mm). At the design point the fan is characterized by the following parameters: R1 rotational speed is $NR1 = 9333$ rpm (100%), corrected R1 tip speed is $U_{tip,cor}=273$ m/s, corrected airflow is $G_{cor}=49.5$ kg/s, total pressure ratio is $\pi^*_f = 1.5$. The general view of the fan with the air intake duct and the flow non-uniformity simulator at the inlet (Section A2) with the nominal nozzle ($D_n=603$ mm) at the by-pass duct outlet is shown in Fig. 1.

Table 1

	1	2	6
M/V, m/s	0.8	100	100
α°	5	15	15
β°	0	0	0
NR1, %	83	54	94
Gcor, kg/s	40.2	24.7	46.2
$q(\lambda_f)$	0.6777	0.4322	0.7701
σ_f	0.940	0.985	0.952
$\Delta\sigma_r$	4.4	3.2	4.2
W	6.0	6.4	4.6

The C-3A test facility is designed for mechanical, aerodynamic and acoustic tests of bypass CRF and straight-flow fan models. The tested fan model is located in the acoustic (anechoic) chamber simulating conditions of a free acoustic field and having the space about 1300 m³ at 6-m distance from the chamber rear wall. The test object mounted at the test facility is shown in Fig.2.

The information-measurement system of the test facility includes 7 workstations intended for monitoring, on-line analysis and recording of all necessary parameters of the test object and main technological systems of the test facility. The test object was properly instrumented to get information on CRF1 aerodynamic characteristics and non-uniform flow in the duct [1-4].



Fig. 2. Test object installed at C-3A test facility

2. Simulation of flow distortion at CRF1 inlet

Calculations of non-uniformity simulators (shading devices) were based on the analysis of total pressure fields at the fan inlet that were found by TsAGI (Moscow region, Zhukovsky) in tests of a powerplant air intake model integrated into the airframe of an advanced aircraft. For non-uniform flow simulation at the CRF1 inlet the following three basic flight conditions were chosen: take-off – $V = 100$ m/s; $\alpha = 15^\circ$, NR1 = 94%, climbing – $M = 0.8$, $\alpha = 5^\circ$, NR1 = 83% and landing – $V = 100$ m/s, $\alpha = 15^\circ$, NR1 = 54%. Flight altitude in these conditions is not high and most of acoustic investigations are provided at this altitude. Table 1 shows parameters describing flow non-uniformity (σ_f - total pressure ratio, $\Delta\sigma_r$ -radial non-uniformity and $W = \Delta\sigma_0 + \varepsilon$ - integral criterion, where $\Delta\sigma_{circumf}$ - circumferential distortion, ε - total pressure pulsation intensity). As an example, Fig. 3 shows a non-uniform total pressure field (isobars in the measurement section at the fan inlet) as drawn for take-off (NR1 = 94 %) based on test results for the air intake model.

For simulation of total pressure fields the C-3A test facility uses flow shading screens. Total pressure fields were divided into zones where changes in σ_f were within 5 %. For each zone a screen with a "live" cross-section that provided a corresponding decrease in total pressure σ_{grid} in the specified operating conditions of the fan was chosen.

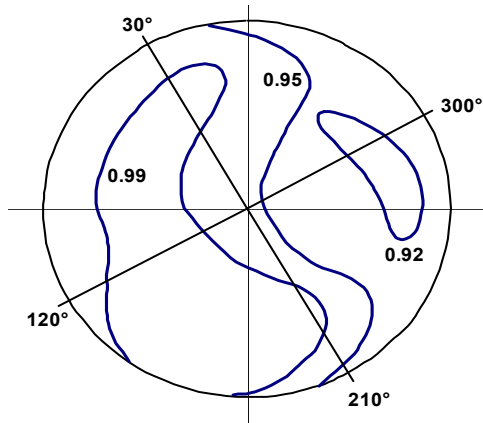


Fig. 3. Total pressure field at the CRF1 inlet at NRI = 94% (TsAGI)

The schematic diagram of grid-screen combinations for simulation of inlet flow non-uniformity in take-off conditions is shown in Fig. 4. The total pressure field is divided into three zones. In Zone 1 outlined by $\sigma=0.99$ isobar the shading screen is not used. The shading screen with $S_{grid}=0.86$ relative "live" cross-section is used in Zone 2 outlined by $\sigma=0.99$ and $\sigma=0.95$ isobars and in Zone 3 outlined by $\sigma=0.95$ isobar and the duct wall. In Zone 3 the screen with $S_{grid}=0.86$ is covered by the screen with the same "live" cross-section - $S_{grid}=0.86$. As a result, total "live" cross-section in Zone 3 is $S_{grid}=0.72$.

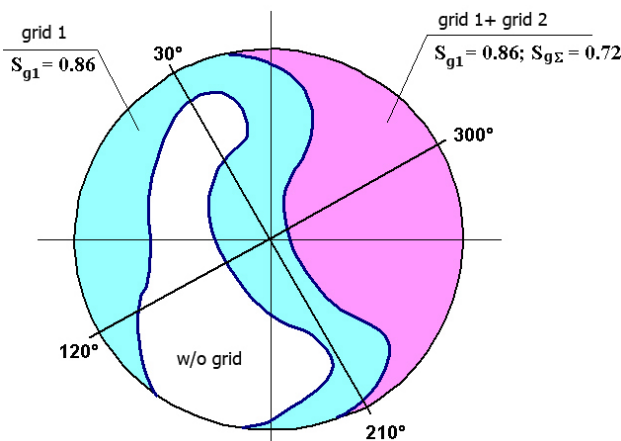


Fig. 4. Schematic of the screen simulator of flow non-uniformity

For simulation of non-uniform flow at the CFR inlet by using the shading screens an intake duct with a special device – the ring with fixed screens - was designed and manufactured. Fig. 5 shows a photo of the fan intake duct with the mounted flow distortion simulator.



Fig. 5. Fan intake duct with the mounted flow non-uniformity simulator

The tests at C-3A test facility showed that total pressure fields found behind the grid-screen simulator, slightly differ in configuration and characteristics from the specified total pressure fields studied in 3 operating conditions. As an example, Fig. 6 shows the total pressure field found at the test facility behind the flow non-uniformity simulator in take-off conditions (NRI = 94%).

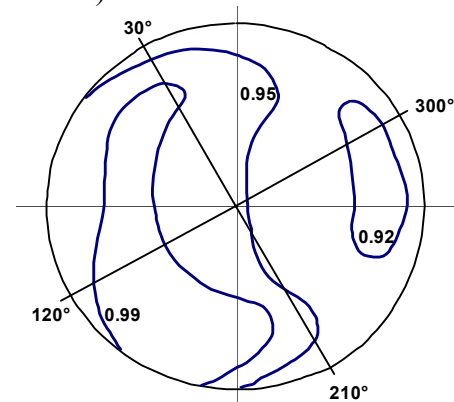


Fig. 6. Total pressure field behind the simulator. NRI = 94%, (C-3A)

3. Test procedure and results

After the test facility startup the average rotational speed was incrementally increased: $N_{av} = (N1+N2)/2 = 50\%, 54\%, 60\%, 80\%, 83\%, 80\%, 90\%, 94\%$ and 95% . Using the throttle valve of the inner duct the nominal $N2/N1$ ratio between rotational speeds was setup. Aerodynamic characteristics of the fan along the operating line under the preset flow non-uniformity at the inlet were measured within the total range of rotational speeds.

In the course of fan tests total flow temperature and total pressure were measured in Section D1 at the aft rotor outlet along the

radius of the flowing passage of the fan by-pass duct at 8 points on the circle as well as static pressure was measured on external and internal walls of the by-pass duct. Based on test results, distributions of the basic fan characteristics (total pressure ratio, π^*_f , adiabatic efficiency η^*_{ad} , and corrected flow velocity, λ) along the radius of the annular duct (by averaging the parameters along the circle) as well as along the duct circumference for 4 radiuses were drawn.

The basic overall aerodynamic characteristics of the experimental fan received in tests with non-uniform air flow at the inlet and the nominal nozzle having 603-mm outlet diameter are shown in Fig. 7 – Fig.10. For comparison, test results with the uniform air flow at CRF1 inlet and nozzles having 603-mm and 595-mm outlet diameters are shown in these graphs. Additionally, results of preliminary calculations are presented. As evident from Fig. 7, values of pressure ratio for CRF1 with uniform and non-uniform air flow at the inlet at the same rotational speed N_{av} are very close. Apparently, the fan choking effect is compensated by a decrease in total pressure coefficient in non-uniform flow at the inlet. Fig. 8 shows $G_{cor}(N_{av})$ dependence. As can be seen, $G_{cor}(N_{av})$ dependence for the fan with the nominal nozzle ($D_n = 603$ mm) at the output and with non-uniform air flow is in good agreement with the same dependence for the fan with the closed nozzle ($D_n = 595$ mm) and with uniform air flow at the inlet. In this case, the non-uniformity simulator decreases total airflow in the fan with the nominal nozzle by 1.0 -1.5 kg/s at the fixed rotational speed, N_{av} .

Fig. 9 and Fig. 10 show the relationships between total pressure ratio, π^*_f , or adiabatic efficiency, η^*_{ad} , and total air flow, G_{cor} , for the tested fan. As shown in Fig. 9, the operating line for the fan with the nominal nozzle ($D_n = 603$ mm) and non-uniform flow at the inlet almost coincides with the operating line of the fan with the closed nozzle ($D_n = 595$ mm) and uniform flow at the inlet. The $\eta(G_{cor})$ curve for the fan with the nominal nozzle and non-uniform flow at the inlet lies 2-5 % below the same dependence for the fan with the same nozzle and uniform flow at the inlet and 0.7-2.5 % below

$\eta(G_{cor})$ dependence for the fan with covered nozzle and uniform flow at the inlet.

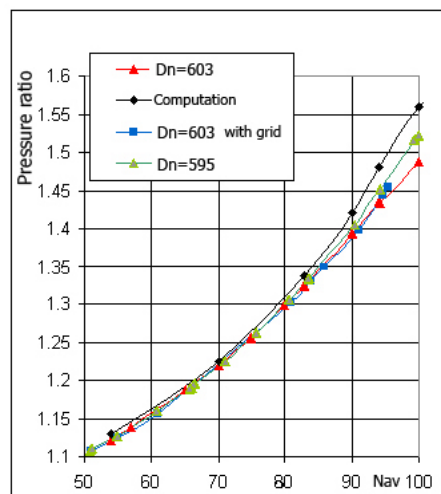


Fig. 7. Pressure ratio as a function of average rotational speed

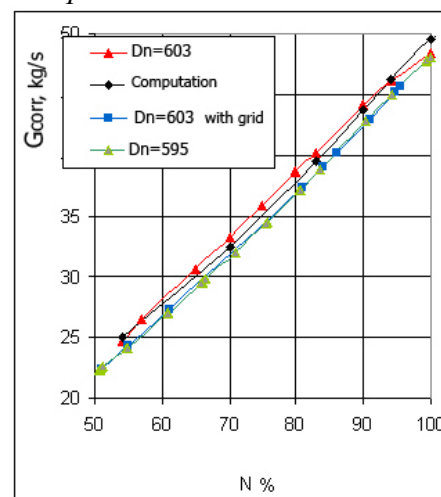


Fig. 8. Total air flow - average rotational speed relationship

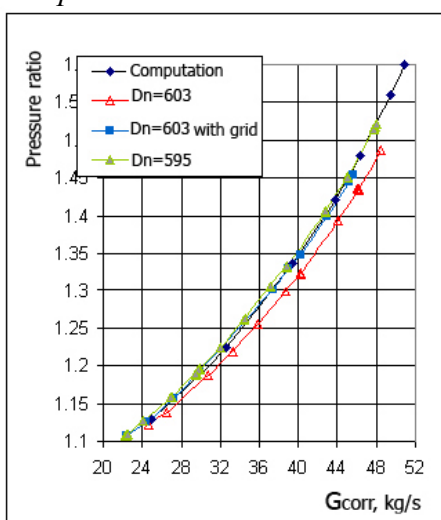


Fig. 9. Total pressure – corrected air flow relationship

NUMERICAL AND EXPERIMENTAL INVESTIGATIONS OF CRF WITH SIMULATION OF FLOW NON-UNIFORMITY IN THE BASIC FLIGHT CONDITIONS

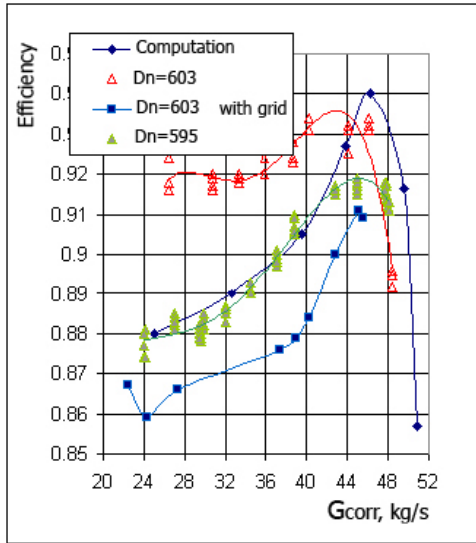


Fig. 10. Adiabatic efficiency – corrected air flow relationship

Fig. 11 – Fig. 14 show distributions of π^*_f , η^*_{ad} , λ , as well as the total flow temperature difference ($T^* - T^*_{inlet}$) along the flow passage radius of the fan by-pass duct at $N_{av}=94\%$. Values of the radius from the fan axis as related to the radius of the external wall of the flow passage are shown on Y-axis in all graphs. The relative radius of the internal (hub) wall is equal to 0.64.

As evident from Fig. 11, an increase in π^*_f up to the values corresponding to π^*_f measured earlier in tests with the covered nozzle and uniform air flow at the inlet (the choking effect) is observed in the flow hub sections ($0.64 < R < 0.85$) at all values of N_{av} . However, only a slight increase in π^*_f is observed in the tip flow section ($0.85 < R < 1$) at $N_{av} = 54 \%$ and $N_{av} = 83 \%$ and even a decrease in π_a close to the external wall at $N_{av} = 94\%$. Therefore it is possible make a conclusion that the effect of the flow non-uniformity on π^*_f is the most noticeable in the tip flow section at the fan outlet and at high rotational speeds.

Fig. 12 shows that the most considerable decrease in fan efficiency (by 11 %) caused by flow non-uniformity at the inlet takes place at all values of N_{av} in the tip flow section at the fan outlet ($0.64 < R < 0.85$) as a result of a strong influence of flow non-uniformity on π_a in this flow area. Efficiency in the flow hub sections ($0.64 < R < 0.85$) is kept constant at small and mean values of N_{av} and even increases by 2% at

high values. Such efficiency behaviour can be accounted for a slight decrease (by 0.5°C at $N_{av}=54 \%$ and $N_{av}=83 \%$) of total temperature in the flow hub sections at the fan outlet. This effect can be clearly observed at $N_{av} = 94 \%$ (by 1.5°C).

Fig. 13 shows distributions of corrected flow velocity at the rotor 2 outlet along the radius. As evident, there is a smooth decrease of flow velocity along the radius - by 6 % at $N_{av} = 94 \%$.

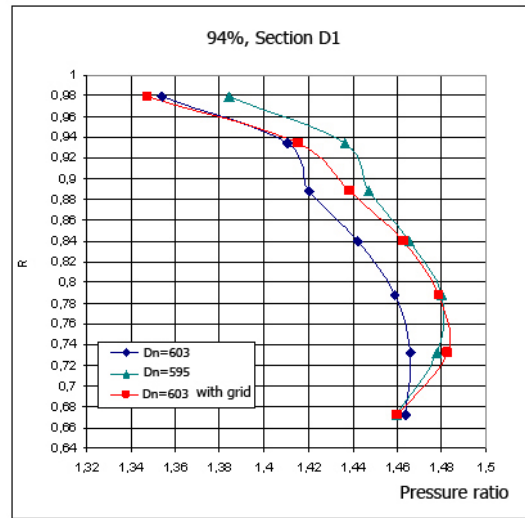


Fig. 11. Distribution of total pressure ratio along the radius at $N_{av} = 94\%$

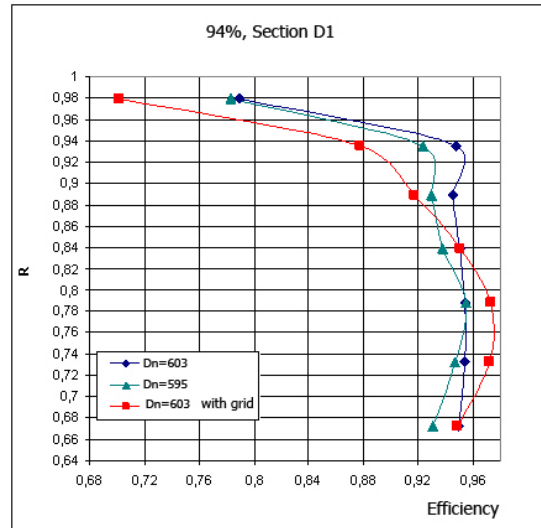


Fig. 12. Distribution of adiabatic efficiency along the radius at $N_{av} = 94\%$

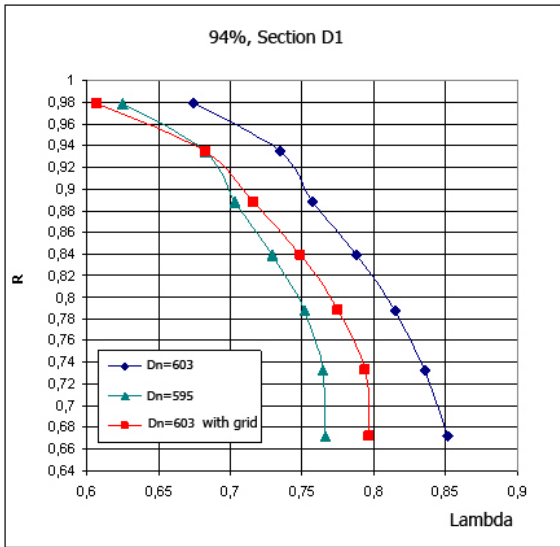


Fig. 13. Distribution of corrected flow velocity at the R2 outlet along the radius at $N_{av} = 94\%$

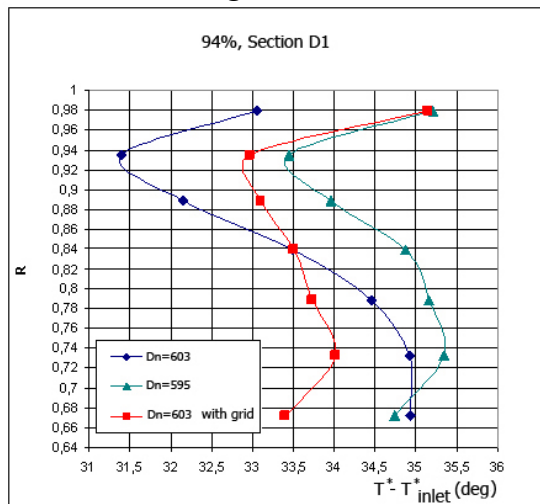


Fig. 14. Distribution of total flow temperature difference at the fan outlet along the radius at $N_{av} = 94\%$

Fig. 15 and Fig. 16 show distributions of π_f^* and fan efficiency along the circle for four radiuses at $N_{av} = 94\%$. Solid lines correspond to test results of the fan with the nominal nozzle and non-uniform flow at the inlet, dash lines - to test results of the fan with the nominal nozzle and uniform flow at the inlet.

It is clear from the curves that at presence of flow non-uniformity at the fan inlet max. values of π_f^* and η_{ad}^* are observed in the hub flow section at the fan outlet within the range of angles from 40° to 200° at all rotational speeds. This flow area at the fan outlet is very similar to the area of zero total pressure losses at the fan inlet.

Some curves in Fig. 15 are drawn above $\eta_{ad}^* = 100\%$ that can be accounted for the fact that total pressure values in flow at the fan outlet in calculations of local pressure ratio are related to a single value - the averaged total pressure at the outlet of the fan inlet non-uniform flow simulator.

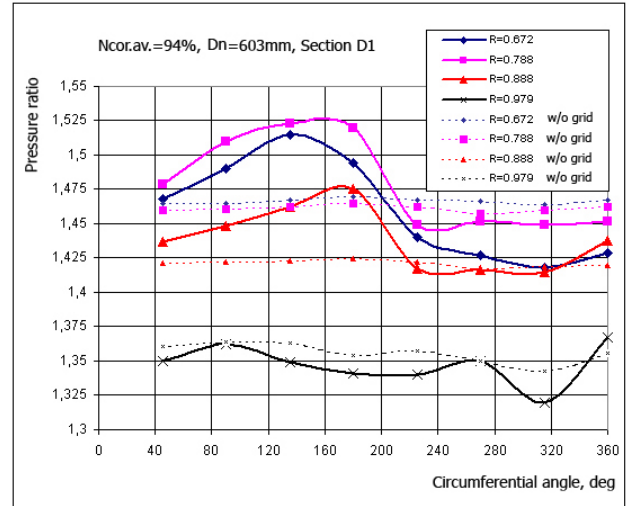


Fig. 15. Distribution of total pressure ratio at the fan outlet along the circle $N_{av} = 94\%$

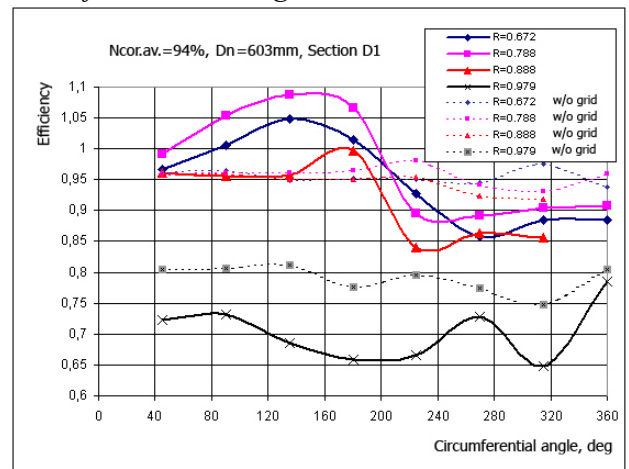


Fig. 16. Distribution of adiabatic efficiency along the circle at $N_{av} = 94\%$

4. Results of numerical modelling

A distinctive feature of numerical investigations of the fan operating conditions with inlet non uniformity is the need for calculations of unsteady flow for all blade channels in each row (10 vs 14 – number of R1 and R2 blades). The solution of non-stationary problem is based on S.K. Godunov's method for solution of gasdynamic problems (implicit finite-difference 2nd order approximation - 3DFS software).

NUMERICAL AND EXPERIMENTAL INVESTIGATIONS OF CRF WITH SIMULATION OF FLOW NON-UNIFORMITY IN THE BASIC FLIGHT CONDITIONS

Standard boundary conditions at the fan inlet and outlet are used in these calculations. The axial flow direction and total parameters are specified in the inlet section and the radial balance condition is specified in the outlet section. It is assumed that application of standard boundary conditions in case of a low level of total pressure non-uniformity is correct and results in a negligible error in computed data.

A finite-difference computational grid containing 70 and 60 cells along the chord of R1 and R2, respectively, is used in calculations. In the circumferential direction there are 111 cells per one blade channel in R1 and 87 cells - in R2. There are 70 cells in radial direction. The finite-difference computational grid has a concentration (crowding) near to solid surfaces that provide an implicit solution of gas sticking to solid surfaces (without wall functions and without account of wall roughness). In total, the finite-difference computational grid contains 18 423 300 cells covering all computational domains (53 blocks). The general view of the grid is shown in Fig. 17.

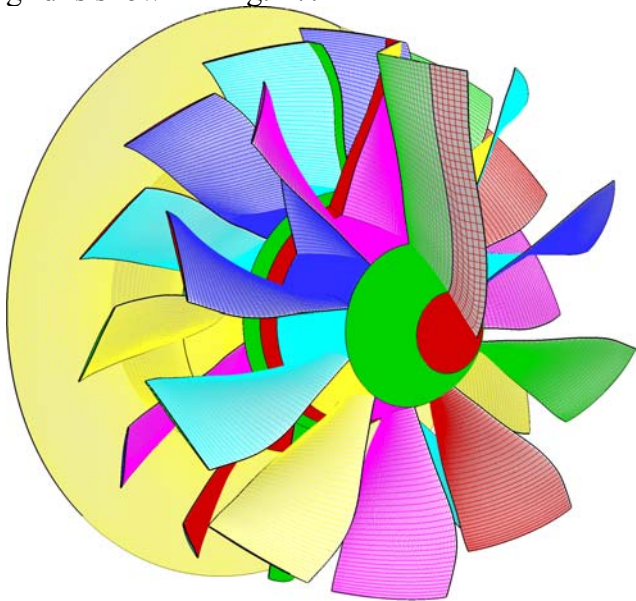


Fig. 17 General view of the finite-difference grid

Numerical modelling of CRF operation with total pressure non-uniformity at the inlet is a three-staged process.

The first (initial) stage includes flow field calculation in mixing plane approximation. This stage is necessary for calculations of initial integral characteristics of the fan and an initial

field for the non-stationary problem statement. Flow calculations for all (10 vs.14) blade channels are provided at this stage.

The second stage covers calculations in non-stationary problem statement with constant total parameters at the fan inlet. This stage is necessary for calculations of non-stationary loads of rotor blades as a result of their interaction and for correction of integral fan characteristics after elimination of an error caused by flow field averaging in the mixing plane approximation (see Fig. 18).

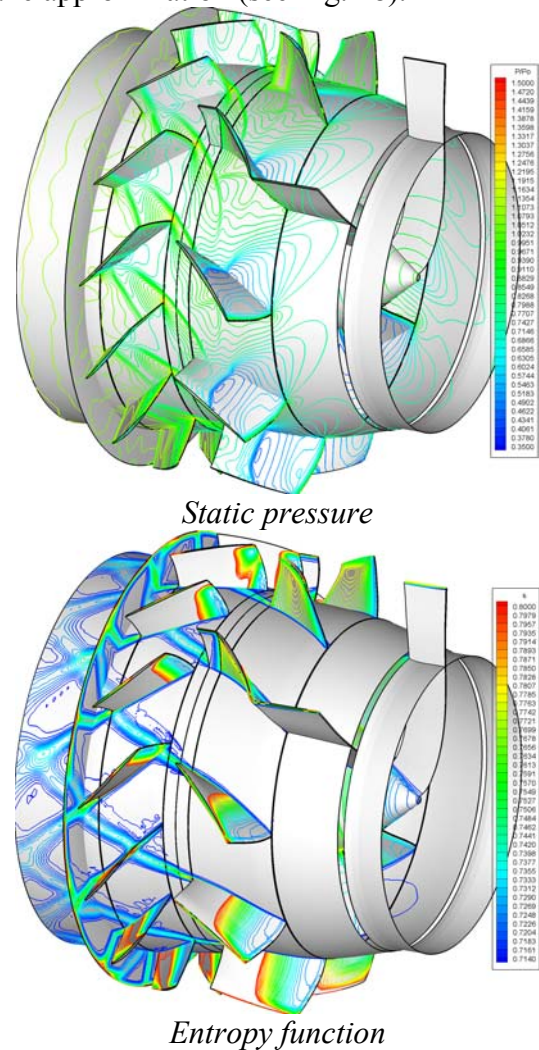
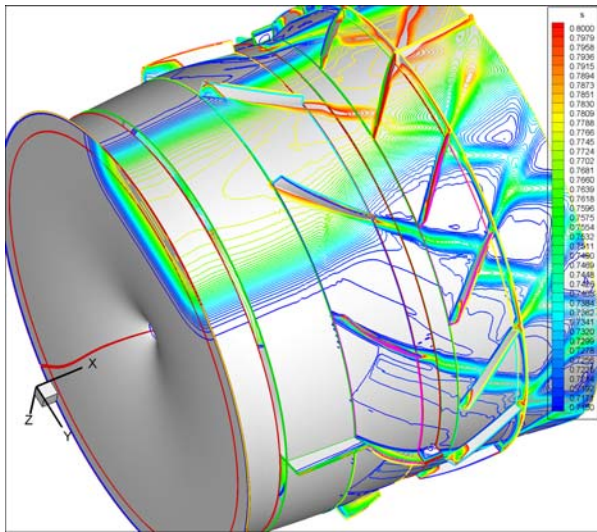


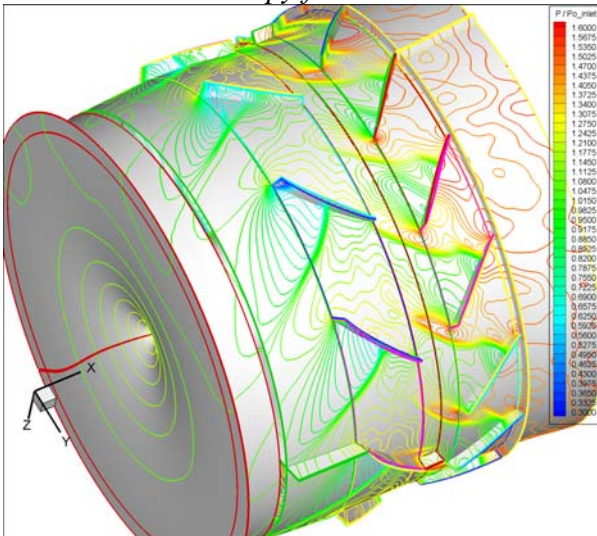
Fig. 18 Instantaneous flow field in the fan model with uniform flow at the inlet

The third stage provides calculations with total pressure non-uniformity at the fan inlet. Non-uniformity is specified as a spot at the tip with a distinctive size close to the cascade spacing and with a wide area of minimal total pressure. The total pressure value in the center

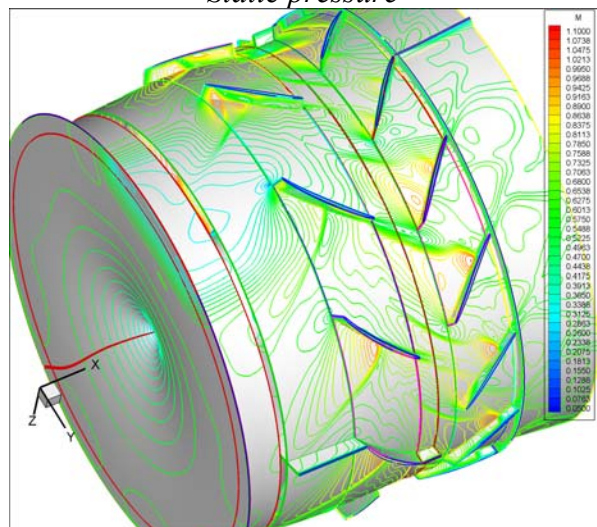
of non uniformity is 20 % less than in the undisturbed flow area at the inlet.



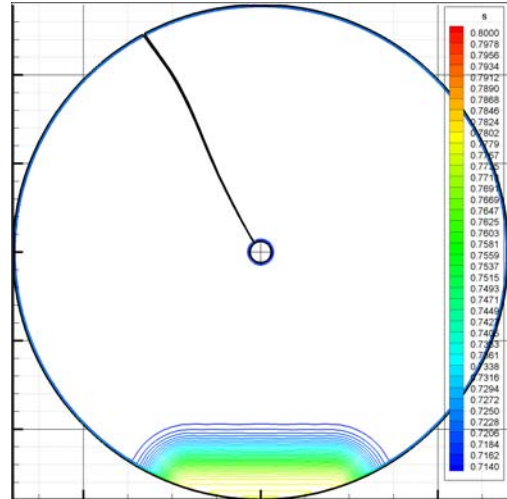
Entropy function



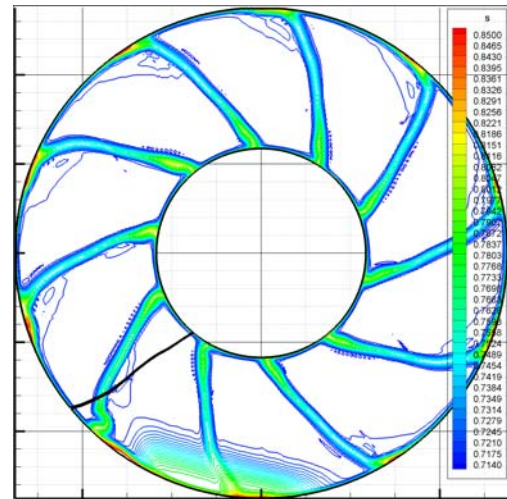
Static pressure



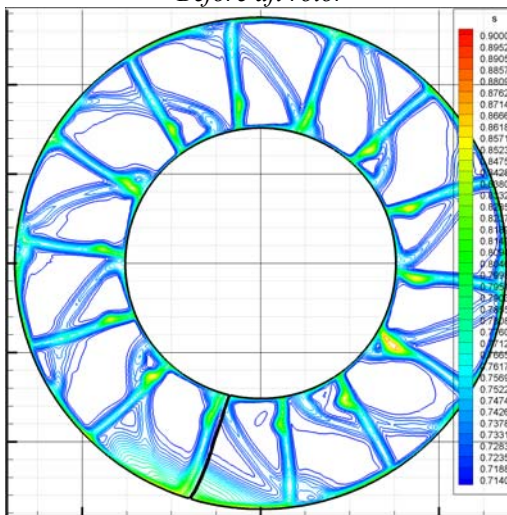
Mach numbers (absolute coordinates)



Inlet section



Before aft rotor



After aft rotor

Fig. 19 Instantaneous flow field in CRF1 fan model with flow non-uniformity at the inlet

Integral characteristics of the fan and pulsations of aerodynamic forces and moments caused by rotor-rotor and blade-flow non-uniformity interactions are found by the calculations.

Comparison and analysis at these three stages give a clear idea of the fan performances within a wide range of operating conditions.

Conclusions

1. The effect of air flow distortion arising at the powerplant inlet of aircraft in three basic operating conditions – take-off, top of climb and landing is studied by numerical and experimental investigations of CRF1 model. Investigations are provided at C-3A test facility equipped with a specially designed simulator of flow non-uniformity at CRF1 inlet.
2. It is shown that total pressure fields measured behind the simulator (grid-screen) at the fan inlet are minor different from the specified total pressure fields in 3 basic flight conditions as to their configuration and characteristics (by 1-2 % for total pressure, σ_b , and radial non-uniformity, $\Delta\sigma_r$).
3. Basic characteristics of the fan along the operating line are found within rotational speeds $N_{av} = 50\% - 95\%$. The experimental data show almost no changes in total pressure ratio, π^*_f , at the same rotational speed for uniform and non-uniform flow at the inlet. In this case total air flow, G_{cor} , in the fan decreases by 1-1.5 kg/s. There is an increase in total pressure ratio by 1.5-2.0 % and a decrease in adiabatic efficiency, η , by 1.0-2.0 % at the same airflow in non-uniform flow.

References

- [1] V.I. Mileshein, S.V. Pankov, V.A. Fateev “Ducted Counter–Rotating Fan Blades Optimization Based on 3D Inverse Problem Solution aiming at fan gasdynamics improvement”. ISABE-2009-1334-Paper, Montreal, 2009.
- [2] J-M. Cailleau. “CRTF fan aerodynamic & acoustic design & concept improvement-Preliminary results”. Snecma, Budapest Congress & World Trade Centre, 9-10 March, Budapest , Hungary, 2009.
- [3] T. Lengyel, C. Voß, T. Schmidt, E. Nicke. Design of a counter rotating fan. an aircraft engine technology to reduce noise and CO2 –emissions. ISABE-2009-1267-Paper Montreal, 2009.
- [4] Jérôme Talbotec, Michel Vernet. Counter rotating fan aerodynamic design logic & tests results. ICAS 2010, Nice, France, Sept. 2010.

Contact Author Email Address

mileshin@ciam.ru

Copyright Statement

The authors confirm that they, and/or their company or organization, hold copyright on all of the original material included in this paper. The authors also confirm that they have obtained permission, from the copyright holder of any third party material included in this paper, to publish it as part of their paper. The authors confirm that they give permission, or have obtained permission from the copyright holder of this paper, for the publication and distribution of this paper as part of the ICAS2010 proceedings or as individual off-prints from the proceedings.